Appl. Phys. A (2016)122:234
DOI 10.1007/s00339-016-9755-x

Applied Physics A
Materials Science & Processing

Comparison of the overall temporal behavior of the bubbles produced by short- and long-pulse nanosecond laser ablations in water using a laser-beam-transmission probe

Ayumu Matsumoto[1] · Ayaka Tamura[1] · Atsushi Kawasaki[1] · Takaya Honda[1] · Peter Gregorčič[2] · Naoya Nishi[1] · Ken-ichi Amano[1] · Kazuhiro Fukami[3] · Tetsuo Sakka[1]

Received: 2 October 2015 / Accepted: 12 February 2016

Abstract We investigate the overall temporal behavior of the bubbles produced by 20-ns- and 100-ns-pulse-duration laser ablations in water using a laser-beam-transmission probe (LBTP). This technique gives the transmission signal attributed to the whole bubble dynamics, including the secondary oscillations, with a single laser shot. Comparing the signals obtained for both pulse durations, the periods of the first oscillation of the bubble are almost the same. Nevertheless, the periods of the subsequent oscillations are significantly different depending on the pulse duration. Such results are obtained by virtue of the LBTP technique.

1 Introduction

Laser-induced breakdown and laser ablation in water can be applied to underwater elemental analysis [1, 2] and synthesis of nanoparticles [3, 4]. However, those are very complex phenomena which are characterized by various interactions [1–4]. It is well known that a cavitation bubble is generated along with a plasma, as well as a shock wave, by laser-induced breakdown in water and laser ablation of submerged solids. The laser-induced bubble repeats expansion and contraction in the scale of a few hundred microseconds, which can be well described by the Rayleigh–Plesset equation [5–9], while the plasma disappears in a few microseconds. The bubble dynamics is quite interesting for fundamental research, while it plays an important role for the underwater elemental analysis [10–17] and the synthesis of nanoparticles [18–25].

The effects of the laser parameters on the laser-induced bubble in bulk water (Vogel et al. [26, 27]) and on the bubble produced by the laser ablation in water (Cristoforetti et al. [10]) have been studied. The behavior of the laser-induced bubble has been mainly studied in the pulse duration ranging from femtoseconds to short-nanoseconds so far [10, 26, 27]. On the other hand, it has been clarified that the relationship between the plasma and the bubble is very important to obtain intense and narrow optical emission spectral lines for the underwater elemental analysis, and the relationship can be controlled by changing the pulse duration in the range from ten to hundred nanoseconds [16, 17]. It has also been clarified that nanoparticles are ejected from the bubble in the liquid at the timing of the bubble collapse during the multiple oscillations [4, 24]. However, the whole bubble dynamics including the secondary oscillations in the case of long nanosecond pulse has not been studied, although some bubble images at the first oscillation have been observed [28].

The bubble dynamics has been investigated mainly by shadowgraph imaging [9–12, 14–21, 24, 25, 28]. Other approaches have also been used, such as Schlieren imaging [29], X-ray radiography [30], high-speed laser stroboscopic videography [31], pressure transducer or piezoelectric hydrophone [9, 32], beam-deflection probe [33–35], and optical transmission techniques [36–38]. In the case of shadowgraph imaging, multiple events are required to

✉ Ayumu Matsumoto
matsumoto.ayumu.78w@st.kyoto-u.ac.jp

Tetsuo Sakka
sakka.tetsuo.2a@kyoto-u.ac.jp

1 Department of Energy and Hydrocarbon Chemistry, Graduate School of Engineering, Kyoto University, Kyoto 615-8510, Japan

2 Faculty of Mechanical Engineering, University of Ljubljana, Aškerčeva 6, 1000 Ljubljana, Slovenia

3 Department of Materials Science and Engineering, Graduate School of Engineering, Kyoto University, Kyoto 606-8501, Japan

capture the whole bubble dynamics. Therefore, the shot-to-shot fluctuation makes it difficult to evaluate the temporal behavior of the bubble accurately. In the case of laser-beam-transmission probe (LBTP), the information of the whole bubble dynamics including the secondary oscillations can be obtained with a single laser shot [36], which makes it easy to evaluate the temporal behavior of the bubble accurately.

In the present work, we examine the bubbles produced by the laser ablation of an Al target in water with the laser pulse durations of 20 and 100 ns using the LBTP technique. Our main aim is to investigate the overall temporal behavior of the bubble produced by the long nanosecond pulse irradiation and the applicability of the LBTP technique for monitoring the laser ablation in liquid.

2 Experimental

Figure 1a shows the side view of the experimental setup for the LBTP measurement. A homebuilt Q-switch Nd:YAG laser (pulsed laser) with the wavelength of 1064 nm, the pulse energy of 6.0 mJ (fixed), the pulse duration of 20 (short pulse) or 100 ns (long pulse), and the repetition rate of 0.1 Hz was used for the ablation. The pulsed laser was focused onto a flat edge of an Al target in ultrapure water in the direction normal to the surface by a plano-convex lens with the focal length of 70 mm. The distance between the water surface and the target surface was 10 mm. The beam waist of the irradiation laser was ~50 µm. The ablation spot was adjusted to be the center of the flat edge. The thickness of the target was 1.0 mm. A He–Ne laser (Uniphase, 1103P-1367) (continuous wave (CW) laser) with the wavelength of 632.8 nm was used as a probe beam. The probe beam was expanded 10 times using a beam expander (Sill Optics, S6ASS0107/121) and transmitted through the interaction area in the direction parallel to the flat edge from a side of the target. The whole light transmitted through the interaction area was collected to a photodiode (Thorlabs, Si amplified detector, PDA10A-EC) by another plano-convex lens. The bandwidth of the detector is from DC to 180 MHz. The distance between the ablation spot and the detector was 2.0 m. The signal of the

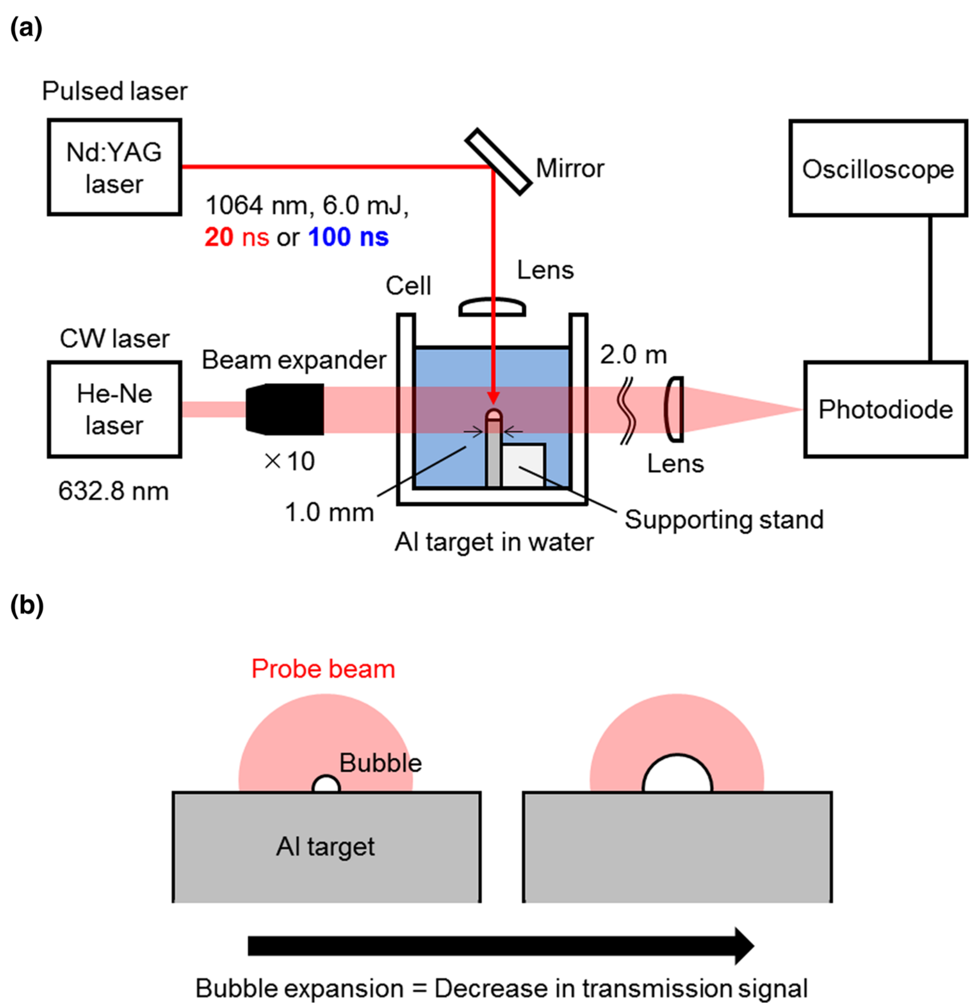

Fig. 1 Experimental setup for laser-beam-transmission probe (LBTP). **a** Side view, **b** Cross-sectional view

detector was recorded by an oscilloscope (Iwatsu, ViewGo II, DS-5654). The bandwidth, the rising time, and the sampling rate of the oscilloscope were 500 MHz, 750 ps, and 1 GS/s, respectively. A trigger signal was taken from another photodiode which detects the reflected light from a beam splitter placed on the optical path of the pulsed laser. The trigger signal was also recorded by the oscilloscope to monitor the pulse duration.

Figure 1b shows the cross-sectional view of the interaction area. The center of the probe beam was intersected with the ablation spot. The spatial radius of the expanded probe beam was ~3.0 mm, which is larger than the maximum radius of the bubble (~1.0 mm [28]). The transmission signal detected by the photodiode reflects the total amount of the transmitted light passed through the region near the target surface. Since the bubble scatters and refracts the probe beam, the transmitted power decreases with the bubble expansion. Therefore, we can obtain the transmission signal containing the information of the expansion and the contraction of the bubble. Note that the detection system of the transmitted light is located far away from the interaction area. Thus, the light scattered or refracted by the bubble is not detected as the transmission signal.

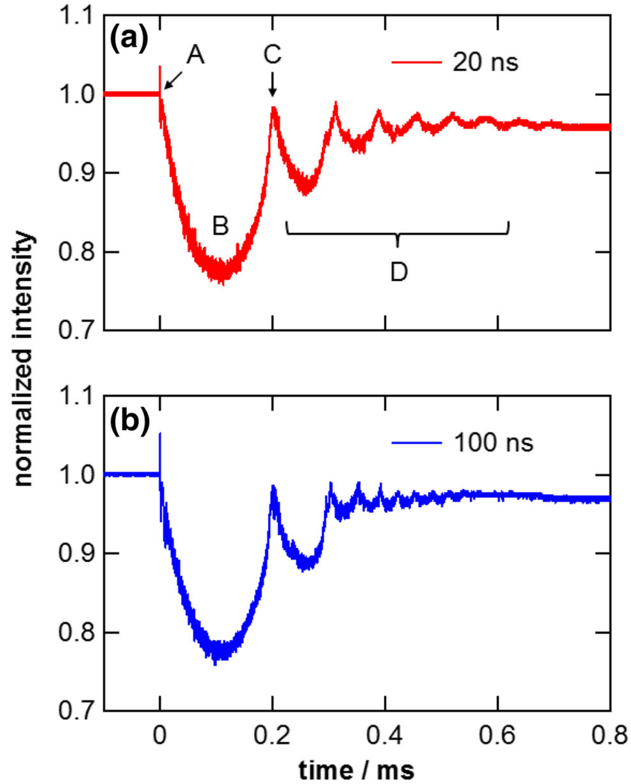

Fig. 2 Typical transmission signals obtained for **a** 20-ns and **b** 100-ns pulse irradiations. The pulse energy is the same (6.0 mJ)

3 Results and discussion

Figure 2a, b shows typical transmission signals obtained for 20- and 100-ns pulse irradiations, respectively. The signals were normalized by the signal voltage acquired before the pulse irradiation. The normalized signals show the typical behavior of the laser-induced bubble. Mark A in Fig. 2a corresponds to the timing of the pulse irradiation. The positive peak is attributed to the plasma emission. Mark B, i.e., the negative peak, appears due to the first oscillation (expansion and contraction) of the bubble. The LBTP signal does not reach zero value, since the spatial radius of the probe beam (~3.0 mm) is larger than the maximum radius of the bubble (~1.0 mm [28]). Mark C shows the timing of the collapse and the re-expansion of the bubble. The time interval between marks A and C is the oscillation period of the first oscillation. Mark D shows the region with several negative peaks that correspond to multiple oscillations of the bubble. The signal did not return to the original position, which is 1.0 in the figure, after the signal attributed to the multiple oscillations is over. This is due to residual matters left near the target surface, which diffuse slowly in water and attenuate the probe beam. Thus, we consider that such a direct current (DC) part of the LBTP signal reflects the particle concentration around the ablation spot after the bubble disappeared.

The positive peak attributed to the plasma emission does not disturb the rest of the LBTP signal. In practice, the plasma emission disappears in a few microseconds [39]. Since the detection system is located far from the point of the plasma generation, the positive peak is very weak and lasts only a few hundred nanoseconds. Such a timescale is extremely shorter than that of the bubble oscillations. Note that we tried to perform similar measurements with a band-pass interference filter which transmits only the light with the wavelength of the probe beam. In this case, the detection of the plasma emission was completely avoided. However, the filter also decreases the intensity of the transmission signal, which made it difficult to observe the multiple oscillations of the bubble. Therefore, the filter was not used in the present experiments.

We cannot discuss the bubble radius straightforwardly from the LBTP signal. This is because the spatial intensity of the probe beam is not uniform and the shape of the bubble at the secondary oscillations is different from an ideal hemisphere. However, the LBTP signal is strongly correlated with the bubble radius. The signal intensity can be theoretically converted to the bubble radius, if the probe laser is well defined [38]. The absolute radius of the bubble, however, is not essential to study the temporal behavior of the bubble. Although the bubble radius is difficult to be measured accurately, the LBTP signal reflects the oscillation period rather precisely.

The overall signals in Fig. 2a, b look very similar at the first glance, while the signals attributed to later oscillations seem to be different. Here, we compare the signals obtained for 20-ns and 100-ns pulse irradiations in detail. It should be noted that we did not change the pulse energy. Figure 3 shows the signals attributed to the first oscillation. Small negative peaks can be observed at the falling edges of signals attributed to the first and second oscillations (see two arrows in Fig. 3). Such peaks are attributed to shock waves, which are induced at the timing of the plasma generation or the bubble re-expansion and propagate in the surrounding water with supersonic speed.

Surprisingly, the signal attributed to the first oscillation did not depend on the pulse duration, although the relationship between the plasma and the bubble during the pulse irradiation is significantly different [17].

Basically, the bubble dynamics is determined by the initial conditions of the bubble. However, it is difficult to determine the initial conditions due to some reasons, e.g., the shape of the nascent bubble is rough and the transient plasma exists in the bubble. It has been reported that nanosecond pulses result in a longer oscillation period of the bubble compared to picosecond pulses [10]. This is explained by the presence or absence of the plasma excitation via inverse bremsstrahlung at the initial stage of the ablation. In the case of nanosecond pulses, the plasma is generated during the pulse irradiation and is excited in the bubble by absorbing the later part of the laser pulse. This increases the temperature of the plasma and gives a momentum for the bubble expansion. In the case of picosecond pulses, the plasma is not excited by the laser pulse, since all the energy is deposited to the target surface before the plasma generation. Comparing the short and long nanosecond pulses, the plasma is rapidly quenched in

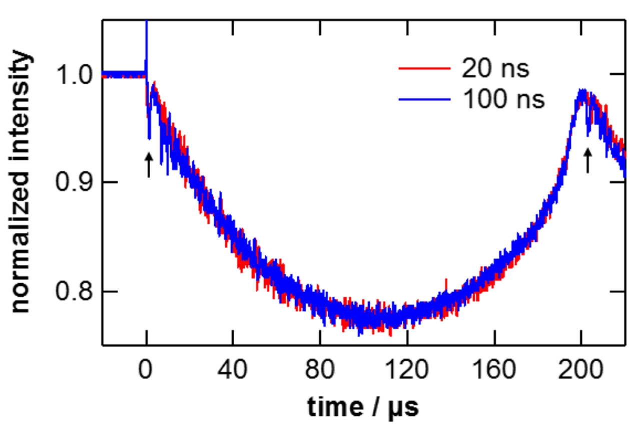

Fig. 3 Comparison of the signals attributed to the first oscillation of the bubble

the case of short pulse, while the high-temperature plasma remains for a longer time in the case of long pulse [17]. Therefore, the oscillation period of the bubble in the case of long pulse is expected to be longer than that of short pulse. However, the period of the first oscillation did not change with the pulse duration in the present experiments (see Fig. 3). We consider that the first oscillation is dominated by the pulse energy rather than the pulse duration, regardless of whether the energy is consumed for heating the target surface or the plasma. In the case of short pulse, a larger number of species are explosively ablated from the target surface and the species are instantaneously excited when the bubble is still small. This gives a higher momentum for the bubble expansion, although the plasma is rapidly quenched. On the other hand, in the case of long pulse, a smaller number of the species are ablated and the species are slowly excited in the expanding bubble. Although the momentum given to the bubble expansion must be smaller immediately after the plasma generation, the rapid quenching of the plasma is suppressed. Thus, the high-temperature plasma persists for a longer time, which has a positive effect on the bubble expansion. Therefore, the periods of the first oscillation can be almost the same regardless of the pulse duration. The bubble expansion may be simply controlled by the pulse energy in the present range of the pulse duration.

Here, we refer to the results of previous shadowgraph measurements that the bubble size at 600 ns after the pulse irradiation does not depend on the pulse duration (30, 50, 100 ns) [17]. The observation of similar bubble sizes at 600 ns supports the present result that the transmission signals attributed to the first oscillation obtained for short and long pulses are almost the same. It is of great interest to observe a nascent bubble during the pulse irradiation using the present technique. But unfortunately, the initial bubble cannot be measured in the present system. Actually, the decrease in the transmission signal attributed to the bubble expansion was observed at several microseconds after the pulse irradiation. Immediately after the pulse irradiation, the positive peak attributed to the plasma emission lasts a few hundred nanoseconds, and successively, the negative peak attributed to the shock wave lasts a few microseconds. Although the band-pass interference filter could block the plasma emission, the shock wave signal cannot be avoided. As for the bubble at the early stage, therefore, we have referred to the results of previous shadowgraph measurements [17].

Figure 4 shows the signals attributed to the second and later oscillations of the bubble. Unexpectedly, the signal attributed to the secondary oscillations significantly depends on the pulse duration, especially from the third oscillation, although the signals attributed to the first oscillation are almost the same. Figure 5 shows the

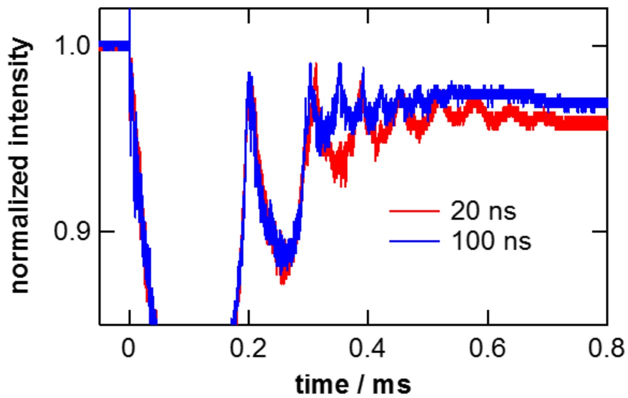

Fig. 4 Comparison of the signals attributed to the subsequent oscillations of the bubble

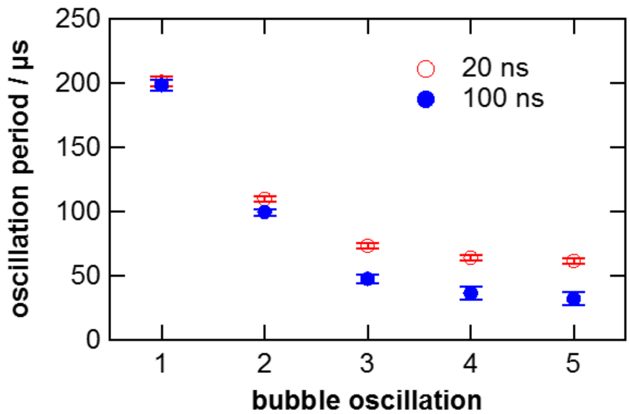

Fig. 5 Comparison of the oscillation period of the bubble plotted in the order of the bubble oscillation. The error bars correspond to the standard deviations of five measurements

oscillation period plotted in the order of the bubble oscillation. The oscillation periods of the later oscillations in the case of long pulse are shorter than that of short pulse. Additionally, we show the averaged signals of five measurements in Fig. 6. The bubble oscillations at the later stage can be clearly seen in the case of short pulse. On the other hand, the bubble oscillations at the later stage in the case of long pulse are averaged out and not seen in this figure, suggesting that the shot-to-shot fluctuation is significant.

Here, we discuss the factors which may affect the later oscillations of the bubble. Considering the fact that the first oscillation does not show significant difference for the irradiations with different pulse durations, the difference observed in the secondary oscillations must be explained in terms of the behavior in the collapse of the precedent bubble. It has been considered that nucleation of particles occurs in the bubble [4, 20, 22, 23]. The particles diffuse with the bubble expansion and aggregate with the bubble contraction. Those are released from inside to outside of the bubble

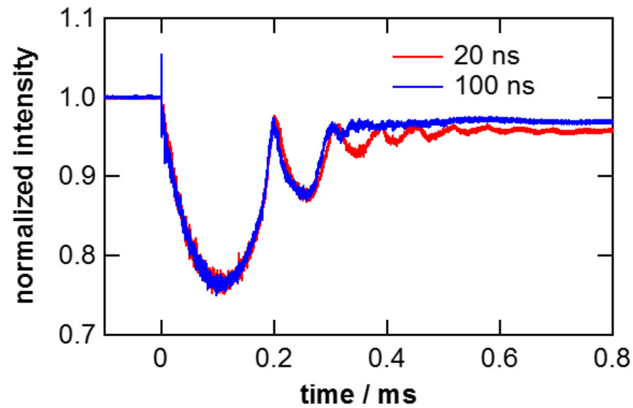

Fig. 6 Comparison of the averaged signals of five measurements

during the bubble collapse and dispersed in water [4, 24]. In the present experiments, we can monitor the particle concentration around the ablation spot after the bubble disappeared from the DC part of the LBTP signal. In the case of short pulse, the intensity of the DC part is relatively low (e.g., see Fig. 6), which means a higher concentration of the particles if we assume that the size distribution of particles is the same. This indicates that a greater amount of the particles exists in the bubble during the multiple oscillations. We believe that the particle concentration in the bubble somehow affects the behavior of the bubble collapse, and hence, the secondary oscillations can be different depending on the pulse duration. Changes in the surface geometry of the target after the pulse irradiation can also affect the behavior of the bubble. Short-pulse irradiation produces a deep crater [40]. The bottom of the crater can be the re-expansion point of the bubble, which can give reproducible oscillations of the bubble. In the case of long pulse, a rough surface without a deep hole is formed [40]. Therefore, the re-expansion of the bubble may be unstable, which causes the shot-to-shot fluctuation. Such a difference may be caused by the relatively high ablation efficiency of the Al target. The bubble size and the oscillation period become smaller and shorter, respectively, with the bubble oscillation. The shape of the bubble at the secondary oscillations is irregular compared with that at the first oscillation [31]. These tendencies agree with the above view that the secondary oscillations are strongly affected by the surface morphology caused by the pulse irradiation.

4 Conclusions

In the present work, we investigated the effects of the pulse duration, namely 20 ns and 100 ns, on the overall temporal behavior of the bubble, which have not been studied enough so far. Particularly, the difference in the secondary oscillations of the bubble has been successfully observed, which is achieved by virtue of the LBTP technique. The signals attributed to the secondary oscillations are considerably different for both pulse durations although those attributed to the first oscillation are almost the same. The results are very interesting because they cannot be explained only by the conventional idea, i.e., the plasma excitation via inverse bremsstrahlung. The present results also indicate that the difficulty in the measurement of the bubble dynamics due to the pulse-to-pulse instability can be overcome by the LBTP technique. Moreover, the LBTP technique is a very appropriate technique for monitoring the laser ablation in liquid, since the signal attributed to the particle concentration has been successfully detected.

Acknowledgments This work was supported by JSPS KAKENHI Grant Number 14J02461.

References

1. A. De Giacomo, M. Dell'Aglio, O. De Pascale, M. Capitelli, Spectrochim. Acta B **62**, 721 (2007)
2. V. Lazic, S. Jovićević, Spectrochim. Acta B **101**, 288 (2014)
3. G.W. Yang, Prog. Mater Sci. **52**, 648 (2007)
4. M. Dell'Aglio, R. Gaudiuso, O. De Pascale, A. De Giacomo, Appl. Surf. Sci **348**, 4 (2015)
5. Lord Rayleigh, Philos. Mag. **34**, 94 (1917)
6. M.S. Plesset, J. Appl. Mech. **16**, 277 (1949)
7. A. Casavola, A. De Giacomo, M. Dell'Aglio, F. Taccogna, G. Colonna, O. De Pascale, S. Longo, Spectrochim. Acta B **60**, 975 (2005)
8. W. Soliman, T. Nakano, N. Takada, K. Sasaki, Jpn. J. Appl. Phys. **49**, 116202 (2010)
9. A. Tamura, T. Sakka, K. Fukami, Y.H. Ogata, Appl. Phys. A **112**, 209 (2013)
10. G. Cristoforetti, M. Tiberi, A. Simonelli, P. Marsili, F. Giammanco, Appl. Opt. **51**, B30 (2012)
11. T. Sakka, A. Tamura, T. Nakajima, K. Fukami, Y.H. Ogata, J. Chem. Phys. **136**, 174201 (2012)
12. V. Lazic, J.J. Laserna, S. Jovićević, Spectrochim. Acta B **82**, 42 (2013)
13. V. Lazic, J.J. Laserna, S. Jovićević, Spectrochim. Acta B **82**, 50 (2013)
14. B. Thornton, T. Sakka, T. Takahashi, A. Tamura, T. Masamura, A. Matsumoto, Appl. Phys. Express **6**, 082401 (2013)
15. B. Thornton, T. Sakka, T. Masamura, A. Tamura, T. Takahashi, A. Matsumoto, Spectrochim. Acta B **97**, 7 (2014)
16. T. Sakka, A. Tamura, A. Matsumoto, K. Fukami, N. Nishi, B. Thornton, Spectrochim. Acta B **97**, 94 (2014)
17. A. Tamura, A. Matsumoto, K. Fukami, N. Nishi, T. Sakka, J. Appl. Phys. **117**, 173304 (2015)
18. T. Tsuji, Y. Tsuboi, N. Kitamura, M. Tsuji, Appl. Surf. Sci. **229**, 365 (2004)
19. T. Tsuji, Y. Okazaki, Y. Tsuboi, M. Tsuji, Jpn. J. Appl. Phys. **46**, 1533 (2007)
20. W. Soliman, N. Takada, K. Sasaki, Appl. Phys. Express **3**, 035201 (2010)
21. A. De Giacomo, A. De Bonis, M. Dell'Aglio, O. De Pascale, R. Gaudiuso, S. Orlando, A. Santagata, G.S. Senesi, F. Taccogna, R. Teghil, J. Phys. Chem. C **115**, 5123 (2011)
22. S. Ibrahimkutty, P. Wagener, A. Menzel, A. Plech, S. Barcikowski, Appl. Phys. Lett. **101**, 103104 (2012)
23. P. Wagener, S. Ibrahimkutty, A. Menzel, A. Plech, S. Barcikowski, Phys. Chem. Chem. Phys. **15**, 3068 (2013)
24. A. De Giacomo, M. Dell'Aglio, A. Santagata, R. Gaudiuso, O. De Pascale, P. Wagener, G.C. Messina, G. Compagnini, S. Barcikowski, Phys. Chem. Chem. Phys. **15**, 3083 (2013)
25. M. Dell'Aglio, R. Gaudiuso, R. ElRashedy, O. De Pascale, G. Palazzo, A. De Giacomo, Phys. Chem. Chem. Phys. **15**, 20868 (2013)
26. A. Vogel, S. Busch, U. Parlitz, J. Acoust. Soc. Am. **100**, 148 (1996)
27. A. Vogel, J. Noack, K. Nahen, D. Theisen, S. Busch, U. Parlitz, D.X. Hammer, G.D. Noojin, B.A. Rockwell, R. Birngruber, Appl. Phys. B **68**, 271 (1999)
28. T. Sakka, S. Masai, K. Fukami, Y.H. Ogata, Spectrochim. Acta B **64**, 981 (2009)
29. V. Lazic, S. Jovićević, M. Carpanese, Appl. Phys. Lett. **101**, 054101 (2012)
30. S. Ibrahimkutty, P. Wagener, T. dos Santos Rolo, D. Karpov, A. Menzel, T. Baumbach, S. Barcikowski, A. Plech, Sci. Rep. **5**, 16313 (2015)
31. R. Tanabe, T.T.P. Nguyen, T. Sugiura, Y. Ito, Appl. Surf. Sci. **351**, 327 (2015)
32. S.J. Shaw, W.P. Schiffers, T.P. Gentry, D.C. Emmony, J. Phys. D Appl. Phys. **32**, 1612 (1999)
33. R. Petkovšek, P. Gregorčič, J. Možina, Meas. Sci. Technol. **18**, 2972 (2007)
34. R. Petkovšek, P. Gregorčič, J. Appl. Phys. **102**, 044909 (2007)
35. P. Gregorčič, R. Petkovšek, J. Možina, Appl. Phys. A **93**, 901 (2008)
36. P. Gregorčič, M. Jamšek, M. Lukač, M. Jezeršek, J. LA&HA **2014**, 14 (2014)
37. M.H. Mahdieh, M. Akbari Jafarabadi, Appl. Phys. A **116**, 1211 (2014)
38. L.F. Devia-Cruz, S. Camacho-López, V.R. Cortés, V. Ramos-Muñiz, F.G. Pérez-Gutiérrez, G. Aguilar. Appl. Opt. **54**, 10432 (2015)
39. H. Oguchi, T. Sakka, Y.H. Ogata, J. Appl. Phys. **102**, 023306 (2007)
40. T. Sakka, H. Oguchi, S. Masai, Y.H. Ogata, Chem. Lett. **36**, 508 (2007)